JOURNAL OF AGRICULTURAL AND FOOD CHEMISTRY

pubs.acs.org/JAFC Article

Universal Nanoplatform for Formaldehyde Detection Based on the Oxidase-Mimicking Activity of MnO_2 Nanosheets and the In Situ Catalysis-Produced Fluorescence Species

Qixia Zhao, Tong Shen, Yujiao Liu, Xiaojun Hu, Wenying Zhao, Zhangyan Ma, Peipei Li, Xiaohua Zhu,* Youyu Zhang, Meiling Liu,* and Shouzhuo Yao

Cite This: *J. Agric. Food Chem.* 2021, 69, 7303−7312 Read Online

ACCESS | Metrics & More | Article Recommendations | Supporting Information

ABSTRACT: Formaldehyde (HCHO) pollution is a scientific problem of general concern and has aroused wide attention. In this work, a fluorometric method for sensitive detection of formaldehyde was developed based on the oxidase-mimicking activity of MnO_2 nanosheets in the presence of *o*-phenylenediamine (OPD). The MnO_2 nanosheets were prepared by the bottom-up approach using manganese salt as the precursor, followed by the exfoliation with bovine serum albumin. The as-prepared MnO_2 nanosheets displayed excellent oxidase-mimicking activity, and can be used as the nanoplatform for sensing in fluorometric analysis. OPD was used as a typical substrate because MnO_2 nanosheets can catalyze the oxidation of OPD to generate yellow 2,3-diaminophenazine (DAP), which can emit bright yellow fluorescence at the wavelength of 560 nm. While in the presence of formaldehyde, the fluorescence was greatly quenched because formaldehyde can react with OPD to form Schiff bases that decreased the oxidation reaction of OPD to DAP. The main mechanism and the selectivity of the platform were studied. As a result, formaldehyde can be sensitively detected in a wide linear range of 0.8−100 μM with the detection limit as low as 6.2×10^{-8} M. The platform can be used for the detection of formaldehyde in air, beer, and various food samples with good performance. This work not only expands the application of MnO_2 nanosheets in fluorescence sensing, but also provides a sensitive and selective method for the detection of formaldehyde in various samples via a new mechanism.

KEYWORDS: *MnO_2 nanosheets, fluorometric method, formaldehyde, Schiff base, oxidase-mimicking activity*

INTRODUCTION

Formaldehyde (HCHO), as a useful chemical material, has been widely applied in resin-manufacturing, synthetic plastic production, leather processing, and preserving tissues.[1] Formaldehyde is active,[2] which can react with olefin in the presence of some specific catalysts. It can also be reduced into methanol under the catalysis of metal or metal oxide, or be transformed into formic acid and carbon dioxide during oxidation.[3] Formaldehyde is also considered as a carcinogenic and mutagenic gaseous pollutant that displays strong interaction with DNA,[4] proteins, and other biomolecules to affect their biological activities.[5] Modern scientific research shows that when the content of formaldehyde indoor is more than 0.1 mg/m^3, there will be peculiar smell and discomfort, stimulating eyes, causing throat discomfort or pain, causing nausea, vomiting, cough, chest tightness, asthma, and emphysema, even leading to death.[6] On the other hand, formaldehyde also plays important roles in keeping the surface color of watery food bright, increasing the toughness and crispness, improving taste, and preventing corrosion. Therefore, formaldehyde can be found in many seafoods, such as shrimp, sea cucumber, pomfret, octopus, cuttlefish, hairtail, squid head, and so on. Formaldehyde is a common preservative because it can coagulate proteins and other impurities. In the traditional brewing process, adding formaldehyde to filter the sediment is very common. In addition, formaldehyde can significantly remove the polyphenols in wort, reduce the color of wort, promote the flocculation and precipitation filtration of protein, significantly improve the abiotic stability of beer, and its cost is relatively low. According to the domestic standard, the maximum content of formaldehyde in beer is about 0.2 ppm (0.2 mg/L). At present, the formaldehyde content of domestic beer generally reaches 1.2 ppm.[7] Excessive intake of formaldehyde will damage the spleen and stomach of the human body, and therefore, it is extremely significant to explore facile and sensitive methods for the detection of formaldehyde in air, beer, and some food samples.

Because formaldehyde has certain reducibility and oxidation ability, it can be determined by spectrophotometry, chromatography, electrochemical methods, and so on.[8−10] However, most of these methods have problems such as bad anti-interference ability and instability, and they can only detect formaldehyde in air or in samples with a higher HCHO concentration. The lower contents of formaldehyde in food samples cannot be detected owing to the lower detection

Received: February 25, 2021
Revised: May 23, 2021
Accepted: May 27, 2021
Published: June 23, 2021

https://doi.org/10.1021/acs.jafc.1c01174
J. Agric. Food Chem. 2021, 69, 7303−7312

sensitivity. Therefore, it is still a huge challenge for the accurate and selective determination of formaldehyde with higher sensitivity.

The rapid development of nanomaterials has brought great opportunities and progress to optical-related fields.[11−14] Due to the particularity of fluorescent nanoplatforms to transform the chemical interaction between molecules into a fluorescence signal, the selective recognition of specific molecules or ions can be realized, which shows the advantages of high sensitivity, simple operation, low cost, and has become a research hotspot in the field of chemical and biological analysis.[15,16] On this respect, the utilization of two-dimensional nanomaterials as the fluorescence quencher and molecular/fluorescence nanomaterial probes as the signal output is considered as a universal strategy for the construction of a fluorescence-sensing system.[17,18] As one of the typical two-dimensional nanomaterials, MnO_2 nanosheets have attracted much attention in fluorescence sensing due to their surface properties, wide absorption band, good redox properties, and good biocompatibility.[19−21] For example, MnO_2-fluorescent polydopamine nanoparticles have been used for the detection of human serum alkaline phosphatase (ALP),[22] and MnO_2−AuNCs can be used for H_2O_2 determination based on fluorescence resonance energy transfer.[23] In many of these MnO_2-based systems, luminescent probes were utilized, whose fluorescence intensity may be greatly affected by the quencher of MnO_2 nanosheets.[24] Moreover, the strategy of using the nanoprobes such as AuNCs and fluorescence polydopamine nanoparticles was relatively complex and their fluorescence properties may be greatly affected by the microenvironment.[25] Another unique property of MnO_2 nanosheets or nanoflakes is their oxidase (OXD)- or peroxidase-like activity, which has also attracted much attention.[26,27] The mimicking properties can be used in construction of colorimetric sensors for the rapid qualitative analysis of various substrates.[28,29] Compared with the colorimetric sensing, fluorescence analysis is more sensitive. Meanwhile, in situ formation of fluorescence species as the signal output based on the nanozyme activity of MnO_2 may be more convenient because there is no need to synthesize fluorescent nanoprobes with higher purity. For instance, by mixing nonfluorescent *o*-phenylenediamine (OPD) with MnO_2 nanosheets that exhibit OXD-like activity, fluorescence species of 2,3-diaminophenazine (DAP) resulting from the catalysis oxidation of OPD by MnO_2 can be obtained, which can be used for the detection of ascorbic acid and ALP.[30] The detection mechanism was based on the fact that AA can reduce MnO_2 nanosheets, resulting in the loss of the OXD-like activity. The in situ formation of fluorescence species is attractive. However, the reductive targets will also cause interference problem. Therefore, the in situ formation of fluorescence species based on the OXD-like activity of MnO_2 nanosheets[31] combined with the utilization of a specific chemical reaction for recognition of special molecules may be employed to develop a nanoplatform with good sensitivity and selectivity, which may be a promising work.

In this work, a nanoplatform with good sensitivity and selectivity for formaldehyde detection was developed using MnO_2 nanosheets with good oxidase activity combined with the in situ-formed fluorescent probes of DAP derived from OPD. The MnO_2 nanosheets can catalyze the oxidation of OPD to DAP with yellow fluorescence in the presence of oxygen; while formaldehyde can react with OPD, which can cause a decrease of the concentration of free OPD that can be catalyzed by MnO_2 nanosheets and reduce the fluorescence intensity of the system. The inhibition of the oxidation of OPD by the specific Schiff base reaction between OPD and formaldehyde accompanied by a decline of the in situ-formed fluorescence species can be utilized for the sensitive determination of formaldehyde. The detection mechanism and the selectivity were investigated in depth, which showed that the in situ-formed fluorescence species enabled the sensitive detection of formaldehyde and the specific chemical reaction showed good selectivity. The detection of formaldehyde in air, beer, and some seafood samples was successfully conducted. This work was different from those reported in the literature which it involved the decline of the nanozyme activity of MnO_2 nanosheets or using the oxidation property of MnO_2. This work not only provides a universal nanoplatform for formaldehyde determination, but also expands the application of MnO_2 nanosheets in food and environmental areas.

EXPERIMENTAL SECTION

Reagents and Materials. Manganese chloride tetrahydrate ($MnCl_2{\cdot}4H_2O$, 99.0%) and OPD (99.0%) were purchased from Tianjin Commio chemical testing Co. Ltd; tetramethylammonium hydroxide (25%) was obtained from Tianjin Guangfu fine chemical research institute (Tianjin, China); bovine serum albumin (98.0%) was obtained from Sigma-Aldrich; and dipotassium hydrogen phosphate (K_2HPO_4, 99.5%), potassium dihydrogen phosphate (KH_2PO_4, 99.5%), formaldehyde (HCHO, 37%), and hydrogen peroxide (H_2O_2, 30 wt %) were provided by Shanghai Wokai biotechnology Co. Ltd. All other chemicals were of analytical grade and used without further purification. Ultrapure water was obtained using a Milli-Q system.

Instruments. The morphology images and energy-dispersive spectrum (EDS) of MnO_2 nanosheets were recorded on a JEM-2100 (JEOL, Japan) transmission electron microscope (TEM). X-ray photoelectron spectra (XPS) were obtained on a K-Alpha 1063 (Thermo Fisher Scientific, British). Fourier transform infrared (FTIR) spectra were collected on a Nexus-870 (Thermo Nicolet, USA). X-ray diffraction (XRD) patterns were obtained using a Rigaku 2500 (Japan) X-ray diffractometer. Fluorescence and UV−vis spectra were obtained on a F-7000 fluorescence spectrometer (Hitachi, Japan) and UV-2450 (Shimadzu, Japan), respectively. The experiments of electrospray ionization mass spectrometry (ESI-MS) were performed on a liquid chromatography−mass spectrometer (LC−MS 8050, Shimadzu, Japan).

Fluorescence Assay of Formaldehyde. The synthesis of single-layer MnO_2 nanosheets was caried out using a procedure similar to that of our previous work[32] and the main process was shown in the Supporting Information (S1). The concentration of MnO_2 nanosheets in the supernatant can be calculated according to the Beer−Lambert Law with a molar extinction coefficient of $9.6 \times 10^3\ M^{-1}\ cm^{-1}$ at 380 nm.[33]

The stock solution of formaldehyde (0.2 mM) was prepared and various concentrations of formaldehyde solution were obtained by dilution of the stock solution. For the detection of formaldehyde, 100 μL of formaldehyde solution with different concentrations was added sequentially to 100 μL of 4 mM OPD, and the mixture was incubated for 50 min at 55 °C. Then, 700 μL of 0.1 M PBS (pH 6.5) and 100 μL of MnO_2 nanosheets aqueous solution (1.74×10^{-2} g/L) were added sequentially with a total volume of 1.0 mL. After the solution was thoroughly mixed and incubated at 55 °C for 70 min, the fluorescence measurements were performed. All the solutions are not pumping of N_2 before detection excepted stated.

Pretreatment of Actual Samples. The formaldehyde sample of the air was obtained as follows: the sampled space was sealed for 24−48 h, 10 L of air in the space was collected with a formaldehyde

https://doi.org/10.1021/acs.jafc.1c01174
J. Agric. Food Chem. 2021, 69, 7303−7312

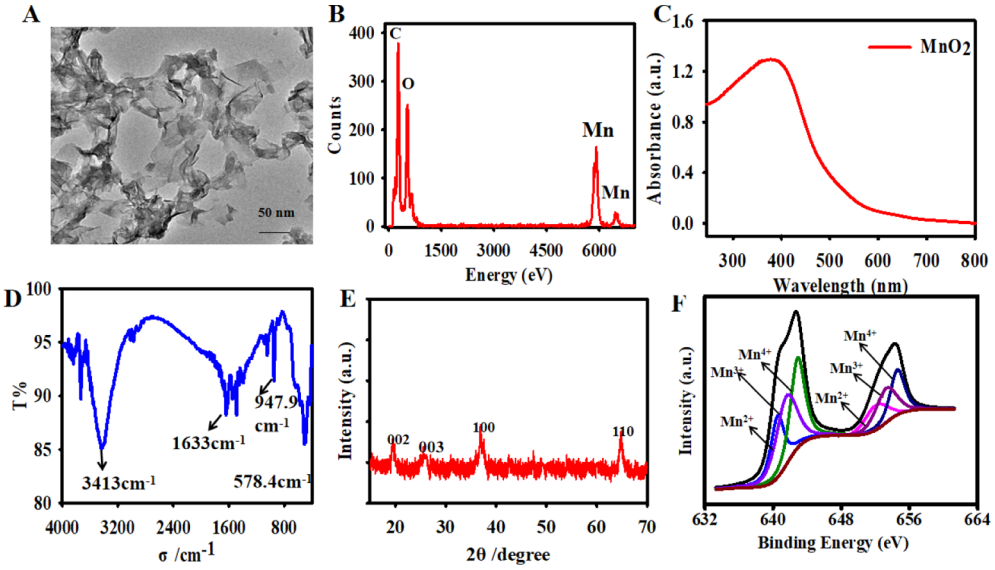

Figure 1. (A) TEM image, (B) EDS, (C) UV−vis, (D) FTIR, (E) XRD pattern, and (F) XPS of MnO_2 nanosheets.

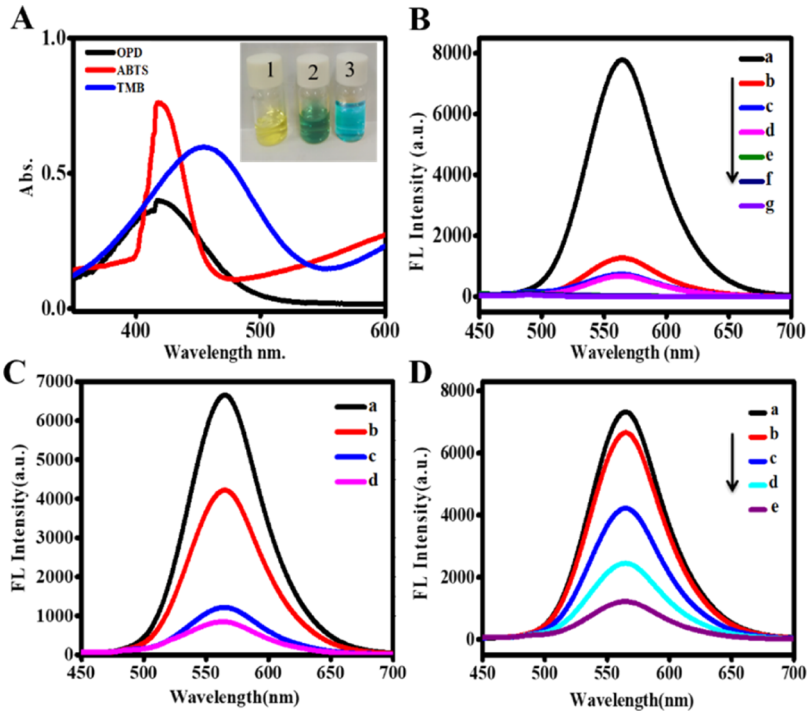

Figure 2. (A) Absorbance of OPD, ABTS, and TMB in the presence of MnO_2 nanosheets [inset, the picture of MnO_2 with OPD (1), ABTS (2), and TMB (3)]. (B) Fluorescence emission spectra of OPD−MnO_2 (a), OPD (b), OPD−MnO_2−HCHO (c), OPD−HCHO (d), MnO_2−HCHO (e), MnO_2 (f), and HCHO (g). (C) Fluorescence emission spectra of OPD−MnO_2 (a), and OPD−MnO_2 pumping with N_2 for 10 min (b); OPD (c), and OPD pumping with N_2 (d). (D) The fluorescence spectra of OPD−MnO_2 with different concentrations of HCHO: 0.0 (a), 10.0 (b), 50.0 (c), 100.0 (d), and 200.0 μM (e).

collection device as shown in the Supporting Information (Figure S1), and an absorbent liquid containing 4 mM OPD (5 mL) was used.

The real sample of beer for formaldehyde detection was obtained as follows: bottled beer (Qingdao, Shandong, China) was purchased from the supermarket in Changsha. The beer bottle was opened after allowing to stand for 2 h to eliminate bubbles, and then took 100 μL sample for formaldehyde detection using a similar procedure to that used for the detection of formaldehyde solution stated above.

Food samples such as frozen golden pomfret (Hainan, China), frozen shrimp (Qingdao, Shandong, China), frozen chicken (Changsha, Hunan, China), and frozen cuttlefish (Zhoushan, Zhejiang, China) were purchased from the supermarket in Changsha. The test solutions were prepared via soaking 2000 mg of the samples in ultrapure water containing 0.1 mol/L HCl aqueous for 5 h. 100 μL of the obtained samples was used for formaldehyde detection.

RESULTS AND DISCUSSION

Characterization of MnO_2. Figure 1A shows the TEM image of MnO_2, which exhibits a typical sheet structure with folds and crinkles. These results may suggest that the MnO_2 nanosheets have a layered structure.[34] Atomic force microscopy (AFM) was conducted as shown in the Supporting Information (Figure S2), and it was found that the thickness of

https://doi.org/10.1021/acs.jafc.1c01174
J. Agric. Food Chem. 2021, 69, 7303−7312

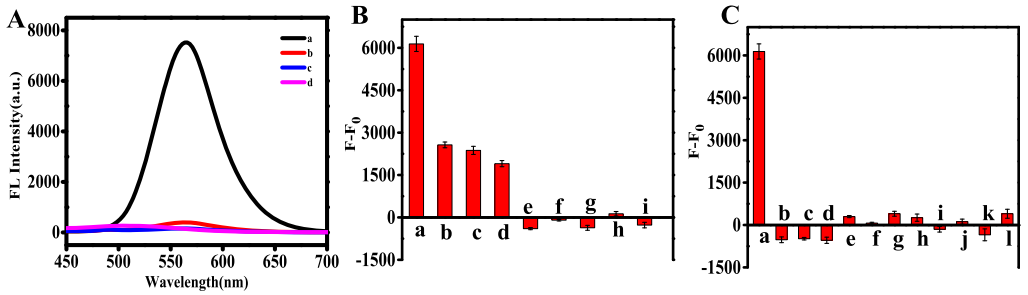

Figure 3. (A) Fluorescence emission spectra of OPD + MnO_2 nanosheets in the presence of H_2O (a), HCHO (b), glutaric dialdehyde (c), and propionaldehyde (d). Concentrations of HCHO, glutaric dialdehyde, and propionaldehyde: 100 μM, OPD: 4 mM; (B) selectivity of HCHO over potential interferences: 10 μM HCHO (a) and 50 μM AA (b), GSH (c), Cys (d), ethanol (e), acetone (f), $NH_3{\cdot}H_2O$ (g), methanol (h), and toluene (i) in the presence of 4 μM OPD. (C) Selectivity of HCHO−OPD−MnO_2 toward metal ions. Concentration of HCHO (a): 10 μM, and concentration of Na^+ (b), K^+ (c), Ca^{2+} (d), Mg^{2+} (e), Al^{3+} (f), Cu^{2+} (g), Cd^{2+} (h), Zn^{2+} (i), Fe^{2+} (j), Fe^{3+} (k), and Pd^{2+} (l): 100 μM. pH 6.5, error bar represents the standard deviation for three times.

the MnO_2 nanosheets in this work was about 2.0 nm, which was in agreement with the literature report.[35] EDS in Figure 1B suggests the existence of Mn and O. The UV−vis spectrum of MnO_2 solution shows a wide absorption band at 300−500 nm with the maximum absorption peak at 380 nm (Figure 1C). The FTIR spectrum in Figure 1D shows the characteristic peaks of MnO_2 nanosheets at 3413, 1633, and 578 cm^{-1}. The peak at 578 cm^{-1} is due to the Mn−O stretching vibrations, while the peak around 1636 cm^{-1} can be attributed to O−H bending vibrations combined with Mn atoms, and the peak at 3413 cm^{-1} is ascribed to O−H bond stretching vibrations, which are in accordance with previous report.[36]

In Figure 1E, the XRD pattern shows four diffraction peaks located at about 18, 26, 36, and 65°, which are indexed to the (002), (003), (100), and (110) of MnO_2. In order to further prove the formation of MnO_2 nanosheets, XPS of the product was collected (Figure 1F). The peak of 641.9 eV is fitted to $2p_{3/2}$ and the peaks of 643.6, 642.3, and 640.9 eV are fitted to Mn^{4+}, Mn^{3+}, and Mn^{2+}, respectively. These results agree well with the XPS patterns of MnO_2. All the above characterizations suggest the successful synthesis of MnO_2 nanosheets.

Properties of MnO_2 Nanosheets and the Feasibility of Detecting HCHO. Using OPD, 2,2′-azino-bis (3-ethylbenzothiazoline-6-sulfonic acid) (ABTS), and 3,3′,5,5′-tetramethylbenzidine (TMB) as the substrates, the oxidase-mimicking activity of the MnO_2 nanosheets was studied. In Figure 2A, it is found that all of the substrates can be catalytically oxidized into their oxidized products accompanied by yellow, green, and blue color, respectively, showing that the MnO_2 nanosheets exhibit OXD-like activity. Using TMB as the typical substrate, the kinetics experiments of OXD activity of MnO_2 nanosheets were performed. By changing the concentration of TMB (Figure S3), the typical Michaelis−Menten plots of OXD mimics can be obtained. The linear regression (for TMB) equation was $y = 0.0073x + 0.1328$ ($R^2 = 0.9927$), and the K_m and V_{max} values for TMB were 0.055 mM and 7.5×10^{-8} Ms^{-1}. Compared with other OXD-like nanocatalysts, larger V_{max} suggests the good catalytic efficiency (Table S1).

As shown in Figure 2A, using OPD as an example, MnO_2 nanosheets catalyze the colorless OPD into yellow DAP with the appearance of a typical absorbance peak at 421 nm. Because the MnO_2 nanosheets show OXD-like activity, they may be utilized as a nanoplatform for the detection of some species that can affect the color reaction of OPD to DAP. Here, formaldehyde was selected as a typical example, which can selectively react with OPD. Figure 2B shows the feasibility of detecting HCHO with MnO_2 and OPD. For the system of OPD + MnO_2 (a) in the presence of O_2, the fluorescence is the largest, which may result from the catalysis of MnO_2 nanosheets to the oxidation of OPD into DAP in the presence of oxygen. The in situ-formed DAP shows excellent fluorescence emission at 560 nm. However, OPD also shows visible fluorescence owing to the small amount of DAP produced in the presence of O_2 (b). However, with the addition of HCHO, the fluorescence of the system OPD + MnO_2 was greatly quenched (c). It is notable that no fluorescence signals appeared for other cases of OPD + HCHO (d), MnO_2−HCHO (e), MnO_2 nanosheets (f), and HCHO (g). It showed that in the presence of HCHO, all cases display a smaller fluorescence intensity owing to the reaction of OPD and HCHO, resulting in the decrease of free OPD. In addition, Figure 2C shows that in the presence of MnO_2 nanosheets, the yellow color of the system (a) is deeper than that without it (c). It can also be seen that upon decreasing the amount of oxygen by pumping N_2 into the solution, the yellow color will become much lighter accompanied by a decline of the fluorescence intensity at 560 nm (Figure 2Cb,d). These results further confirm that the MnO_2 nanosheets can catalyze the OPD oxidation into DAP with a yellow color in the presence of oxygen, owing to their OXD activity. Therefore, the in situ-produced oxidation product of DAP is closely related to the catalysis of the MnO_2 nanosheets for their OXD activity, while the interaction of OPD and HCHO can decrease the concentration of the resulting oxidized product of DAP with a decline in fluorescence intensity. Figure 2D suggests that the fluorescence intensity reduced gradually with the increase of HCHO concentration. These results may be attributed to the aldehyde group that can react with the amino group of OPD to form Schiff bases and inhibit the further formation of DAP with a decrease of the fluorescence intensity of the system. These suggested that the fluorescence sensing of HCHO based on MnO_2 + OPD is reliable. To this end, the in situ-produced oxidation product of DAP based on the oxidase-mimicking activity of MnO_2 nanosheets combined with the specific reaction of HCHO to OPD can be utilized as a sensitive fluorescence-sensing platform for HCHO.

Mechanism and Selectivity Study. The fluorescence quenching of the system is ascribed to the decrease of the concentration of DAP, which is affected by the catalysis of MnO_2 nanosheets and HCHO. To further confirm the role of MnO_2 nanosheets and the mechanism, we conducted the fluorescence of the system OPD + MnO_2 nanosheets with

https://doi.org/10.1021/acs.jafc.1c01174
J. Agric. Food Chem. 2021, 69, 7303−7312

Scheme 1. (A) Schematic Presentation of the Synthesis of MnO_2 Nanosheets; (B) Detection of HCHO on the Basis of the Oxidase-Mimicking Property of MnO_2 Nanosheets and the In Situ Formation of Fluorescence Species of DAP; (C) Photographs of Real Samples (Beer, Frozen Golden Pomfret, Frozen Shrimp, Frozen Chicken, and Frozen Cuttlefish).

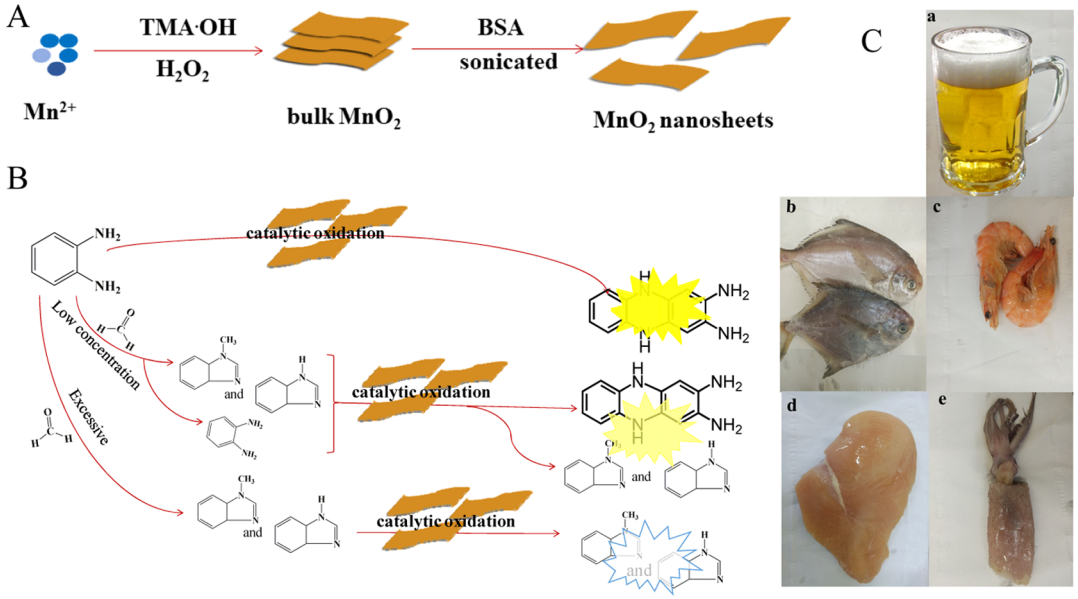

different amounts of O_2. As shown in Figure S4, the fluorescence response is greatly changed in the case of pumping of N_2. After pumping of N_2 for 30 min, the color of the solution becomes much lighter accompanied by a decline of the characteristic peak of DAP even in the presence of the same concentration of MnO_2 nanosheets. However, there is a small peak at 560 nm because a small amount of OPD was oxidized by O_2 that can display a fluorescence response. In contrast, in the presence of enough O_2, an obvious characteristic peak of DAP appeared with strong fluorescence at 560 nm. This is because a large amount of O_2 was eliminated when pumping N_2 that the full oxidation of OPD cannot take place. The amount of the produced DAP and the color as well as the absorbance of the system indirectly suggest the transformation of OPD into DAP was greatly related to the amount of O_2 and the catalyst of MnO_2 nanosheets. Therefore, these results directly indicate that the oxidant is O_2 not MnO_2 nanosheets, which may indirectly reflect the MnO_2 nanosheets acted as the oxidase-mimicking catalyst. The TEM of the MnO_2 nanosheets after the catalysis reaction was also conducted (Figure S5), which shows the sheet structure and further indicates that there was no redox reaction for MnO_2 nanosheets in this system.

The OXD-like activity of MnO_2 nanosheets greatly affects the oxidation of OPD, while HCHO can react with OPD to form stable Schiff bases with a decrease of the amount of free OPD that can be oxidized by MnO_2 nanosheets. To further investigate this mechanism, several aldehydes such as glutaric dialdehyde and propionaldehyde containing a −CHO group were also selected for comparison. It was found in Figure 3A that the fluorescence intensity decreased obviously in all cases, which proved the above mechanism. Considering the high sensitivity and good selectivity of the sensing platform of the OPD + MnO_2 nanosheets to aldehydes, the in situ-formed fluorescence species-based strategy can be utilized for the detection of all kinds of aldehydes. It is reported that the concentration of HCHO is much higher than those of other aldehydes in air and food samples, and the platform may be a good choice for HCHO detection.

In addition, the possible products of the system during the reaction were collected and identified by fluorescence (Figure S6) and ESI-MS (Figure S7). The Schiff base compounds were formed owing to the reaction of HCHO and OPD; however, it is hard to separate the two Schiff bases. It can be detected simultaneously in the fluorescence spectrum, which shows no obvious fluorescence (Figure S6), and this result and the phenomenon are different from those of OPD and DAP. DAP showed stronger fluorescence, while OPD displayed very weak fluorescence owing to the small amount of DAP that was oxidized by the oxygen in the solution (Figure S6). The Schiff bases formed between HCHO and OPD can be further proved by ESI-MS. It was deduced that the two Schiff base products of 1-methylbenzimidazole and benzimidazole in Scheme 1 appeared in the characteristic m/z peaks at 133.00 and 119.00, which could be 1-methylbenzimidazole ($[M + H]^+$) and benzimidazole ($[M + H]^+$), respectively (Figure S7). All these results suggested that the HCHO and OPD reacted to form Schiff bases, which will further affect the production of the fluorescence species of DAP.

Overall, the detection strategy is based on the oxidase-mimicking activity of MnO_2 nanosheets, and the detection is greatly related to the inhibition of the amount of chromogenic substance not the change of the nanozyme. Therefore, the detection mechanism was different from those of the traditional MnO_2 nanosheet-based fluorescence nanoplatforms that use MnO_2 nanosheets as the quencher or the inhibitor of the OXD-like activity of MnO_2 nanosheets. The OXD-like activity of MnO_2 nanosheets as well as the specific Schiff base reaction are of great novelty and may be expanded to other nanozyme systems.

Though other aldehydes show interference for the detection of HCHO, the amount of HCHO in the environmental condition and foods samples is much higher than those of others. Therefore, the sensitive and selective detection of HCHO in air or foods can be realized via the nanoplatform

https://doi.org/10.1021/acs.jafc.1c01174
J. Agric. Food Chem. 2021, 69, 7303−7312

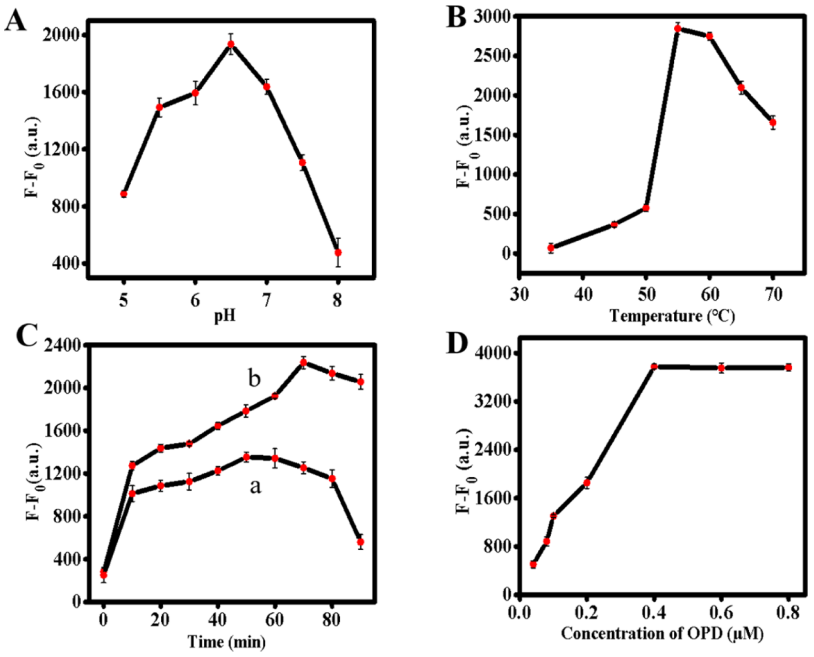

Figure 4. Effect of (A) pH, (B) temperature, (C) reaction time [(a) HCHO reacted with OPD; (b) OPD transformed into DAP on the catalysis of MnO_2 nanosheets], and (D) concentration of OPD for detection of HCHO. Conditions: 100 μL HCHO, 700 μL PBS (0.1 M), 100 μL MnO_2 (1.74×10^{-2} g/L), and 100 μL OPD (0.4 mM) except D with various concentrations of OPD.

based on OPD + MnO_2 nanosheets. To further prove the selectivity for HCHO, some possible interfering molecules in the air environment including AA, GSH, Cys, ethanol, acetone, ammonia, methanol, and toluene with a concentration of 100 μM were chosen for study under the same conditions. The results are shown in Figure 3B, suggesting good selectivity of the sensing platform for the detection of HCHO. The reductive molecules such as AA and GSH may react with the MnO_2 nanosheets via the redox reaction and then destroy the OXD-like activity of MnO_2 nanosheets (as shown in Figure 3B), which make the construction of the detection nanoplatform difficult. Therefore, all the reducing agents need to be oxidized to eliminate their redox reaction to MnO_2 nanosheets. The reductive molecules such as AA and GSH are easy to be oxidized by oxygen at room temperature, while HCHO is difficult to be oxidized in air below 100 °C. Therefore, a simple way to oxidation of AA and GSH is pumping of O_2 in the solution to eliminate the interferences from them. The results shown in Figure S8 confirmed this. In the presence of AA or GSH, the color of the system of MnO_2 nanosheets and OPD is much lighter, and the fluorescence is greatly declined (Figure S8A). This was resulted from the oxidation−reduction reaction of AA or GSH to MnO_2 nanosheets, which can hamper the oxidase-mimicking activity of MnO_2 nanosheets for the catalysis of OPD. However, after the solution of AA or GSH pumping of oxygen for about 30 min, the color reaction of MnO_2 nanosheets and OPD is deeper than that of without pumping of oxygen (Figure S8B). This result suggests that AA or GSH can be oxidized by oxygen, and then they will not affect the mimicking activity of MnO_2 nanosheets. Figure S8C shows the detection of HCHO in the presence of AA or GSH. It can be found that the oxidation of GSH (c) and AA (d) via pumping of O_2 was similar to that of HCHO−OPD−MnO_2 (b), while greatly different from the case of without pumping of O_2 (e and f). Hence, the interferences can be effectively eliminated by pumping of oxygen before detection. To explore the potential application of HCHO in real solution samples, various ions including Mn^{2+}, Mg^{2+}, Fe^{2+}, Al^{3+}, Ca^{2+}, Cu^{2+} etc., with a concentration of 100 μM, were also investigated (Figure 3C). A slight response in these cases further suggests the good selectivity of MnO_2−OPD to HCHO.

Optimization of Assay Conditions. To obtain the optimal experimental conditions, reaction time, pH, temperature, and concentration of OPD were investigated. pH is a crucial detection factor, and the optimal condition was obtained when the pH value was 6.5 (Figure 4A). Reaction temperature affects the reaction speed and the stability of reactions, and is also an important factor for detection. As shown in Figure 4B, 55 °C is the optimal reaction temperature. Reaction time is also an important factor for the fluorescence intensity, and 50 min is the most suitable time for the reaction of OPD and HCHO, and 70 min is excellent for the assay of the catalysis reaction of OPD into DAP in the presence of MnO_2 nanosheets (Figure 4C). The concentration of OPD is also important for the detection, and the optimal condition was obtained when the concentration of OPD was 0.4 mM (Figure 4D).

Fluorescence Detection of HCHO. Different concentrations of HCHO were added to the OPD solution with a fixed amount of MnO_2 nanosheets under the optimal assay conditions. Figure 5A shows that the fluorescence at 560 nm is sensitive to HCHO. Simultaneously, the fluorescence intensity gradually decreased with the concentration of HCHO. The fluorescence intensity was linearly related to the HCHO concentration in the range of 0.8−100.0 μM, while further increase the concentration did not result in the obvious decline of fluorescence intensity. This may be because the concentration of OPD is constant in the experiment, whose reaction sites were also constant. When all sites reacted with HCHO, further addition of HCHO did not affect the fluorescence of the system. As a result, the linear relationship can be shown as $F_0 - F = 84.198[\mathrm{HCHO}] + 65.596$ with $R^2 = 0.9970$ (Figure

https://doi.org/10.1021/acs.jafc.1c01174
J. Agric. Food Chem. 2021, 69, 7303−7312

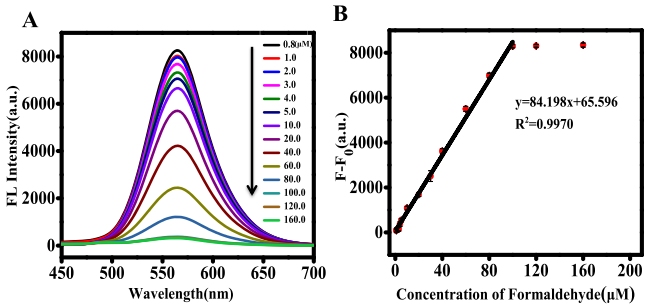

Figure 5. (A) Fluorescence of OPD + MnO_2 with different concentrations of HCHO (0.8, 1.0, 2.0, 3.0, 4.0, 5.0, 10.0, 20.0, 40.0, 60.0, 80.0, 100.0, 120.0, and 160.0 μM). (B) Linear relationship between (F_0−F) and HCHO in (A). Detection conditions: 100 μL HCHO with various concentrations, 700 μL PBS (0.1 M, pH 6.5), 100 μL MnO_2 (1.74×10^{-2} g/L), and 100 μL OPD (0.4 mM).

5B), where F_0 and F represent the fluorescence intensities of MnO_2−OPD in the absence and presence of HCHO, respectively. The detection limit of this experiment is as low as 6.2×10^{-8} M (S/N = 3). The detection performance for HCHO was compared with those reported in the literature, as shown in Table 1, which indicates that the proposed strategy

Table 1. Comparison of Detection of HCHO in this Paper with the Literature

sensing material	method	linear range (μM)	detection limit (μM)	refs
3D core−shell In_2O_3 @SnO_2	electrochemical	0.33−33.3	0.33	37
probe TP-FA	fluorescence	0−600	0.51	38
$FASnI_3/SnO_2$/Pt-240	electrochemical	10−333	2.17	39
fluorescence dye	fluorescence	0−270	6	40
TPE	fluorescence	0−40	1	41
PDA/HMSSs	electrochemical	3−990	3	42
CNTs−Fe_3O_4	electrochemical	1.6−16	1.6	43
Ag nanoclusters and TR	UV−vis	30−50	27.99	44
MnO_2 nanosheets	fluorescence	0.8−100	0.062	this work

displays superior performance owing to the sensitive reaction of the in situ formation of DAP via the oxidase-mimicking activity of MnO_2 and the specific interaction of HCHO with OPD. These results demonstrate that the MnO_2-based fluorescence platform can be applied for HCHO detection in real samples.

Real Sample Detection. The obtained HCHO samples were determined using the same detection process as above. As shown in Table 2, the concentration of HCHO in the sampled space is calculated to be 0.1096 mg/m^3 (0.73 μM), which is higher than the standard limit of the indoor HCHO concentration of 0.08 mg/m^3 according to the national standard.[6] Using the standard additional method for the detection, the recovery is between 95.2−101.5%, indicating the method is reliable. Therefore, the proposed method can provide helpful information regarding indoor air quality.

The concentration of HCHO in the detected beer sample is 0.43 mg/L (14.3 μM), which is lower than the HCHO concentration limit of 2 mg/L stipulated by the national standard.[45] The formaldehyde concentrations in frozen golden pomfret, frozen shrimp, frozen chicken, and frozen cuttlefish

Table 2. Determination of HCHO in Real Samples of Air, Beer, and Some Frozen Foods

sample	added (μM)	detected (μM)	recovery (%)
air	0.0	0.73	
	5	5.49	95.2
	20	20.11	96.9
	60	61.61	101.5
beer	0.0	14.30	
	5	19.43	102.7
	20	33.76	97.3
	60	72.32	96.7
frozen golden pomfret	0.0	31.60	
	1.0	32.57	97.0
	20	51.24	98.2
	60	93.34	102.9
frozen shrimp	0.0	34.30	
	1	35.32	102.0
	20	54.28	99.9
	60	96.82	104.2
frozen chicken	0.0	29.90	
	1	30.93	103.0
	20	49.40	97.5
	60	89.42	99.2
frozen cuttlefish	0.0	38.90	
	1	39.94	104.0
	20	58.72	99.1
	60	97.34	97.4

are 31.60, 34.30, 29.90, and 38.90 μM, respectively, which are lower than the HCHO concentration limit stipulated by the national standard.[46] To further confirm the accuracy of the method, the standard additional method was also used for the detection of beers and sea foods, with the recovery at 96.7−104.2%, respectively.

Besides, the proposed method was also applied for the synthesized sample detection, which contained AA/GSH and HCHO. The results are given in Table S2, and recovery is satisfactory, which means that the method is reliable and can be utilized as a universal method for HCHO detection in various real samples.

In summary, a sensitive and selective fluorometric strategy for HCHO detection based on the MnO_2−OPD nanoplatform was constructed. The MnO_2 nanosheets with oxidase-mimicking activity can catalyze the oxidation of OPD in situ formation of luminescence DAP with the emission peak at 560 nm. While HCHO can react with OPD with the production of Schiff bases decreasing the chance of oxidation of OPD to DAP, which can greatly affect the fluorescence intensity of the system. Based on this mechanism, the quantitative detection of HCHO was realized. The main advantages of the work include: (1) MnO_2 nanosheets with high efficiency and oxidase-mimicking activity can effectively catalyze the oxidation of OPD to DAP in the presence of oxygen; (2) the in situ-formed DAP can provide stable fluorescence that avoids the complex additional synthesis of fluorescent probes; (3) the specific Schiff base reaction of OPD to HCHO promises the high selectivity of the nanoplatform. Therefore, the new detection mechanism, a highly sensitive and selective strategy, and universal applicability in real samples endow MnO_2 nanosheets with great potential for the detection of

https://doi.org/10.1021/acs.jafc.1c01174
J. Agric. Food Chem. 2021, 69, 7303−7312

formaldehyde in other environmental, food, and biological systems.

■ ASSOCIATED CONTENT

Supporting Information

The Supporting Information is available free of charge at https://pubs.acs.org/doi/10.1021/acs.jafc.1c01174.

Process of the preparation of MnO_2 nanosheets; the formaldehyde collection device; AFM of MnO_2 nanosheets; kinetics experiments of the oxidase-mimicking activity of MnO_2 nanosheets; TEM of MnO_2 nanosheets after the catalysis reaction; confirmation of Schiff base compounds by fluorescence and MS; reaction of MnO_2 nanosheets and OPD in the absence and presence of AA or GSH; comparison of the OXD-like activity of MnO_2 nanosheets with that of other nanozymes; and detection of HCHO using the synthesized samples(PDF)

■ AUTHOR INFORMATION

Corresponding Authors

Xiaohua Zhu − *Key Laboratory of Chemical Biology & Traditional Chinese Medicine Research (Ministry of Education, China), College of Chemistry and Chemical Engineering, Hunan Normal University, Changsha 410081, PR China*; Email: zhuxiaohua@hunnu.edu.cn

Meiling Liu − *Key Laboratory of Chemical Biology & Traditional Chinese Medicine Research (Ministry of Education, China), College of Chemistry and Chemical Engineering, Hunan Normal University, Changsha 410081, PR China*; orcid.org/0000-0002-1506-1143; Email: liuml@hunnu.edu.cn, liumeilingww@126.com

Authors

Qixia Zhao − *Key Laboratory of Chemical Biology & Traditional Chinese Medicine Research (Ministry of Education, China), College of Chemistry and Chemical Engineering, Hunan Normal University, Changsha 410081, PR China*

Tong Shen − *Key Laboratory of Chemical Biology & Traditional Chinese Medicine Research (Ministry of Education, China), College of Chemistry and Chemical Engineering, Hunan Normal University, Changsha 410081, PR China*

Yujiao Liu − *Key Laboratory of Chemical Biology & Traditional Chinese Medicine Research (Ministry of Education, China), College of Chemistry and Chemical Engineering, Hunan Normal University, Changsha 410081, PR China*

Xiaojun Hu − *Hunan Institute of Food Quality Supervision Inspection and Research, Changsha 410111, PR China*

Wenying Zhao − *Hunan Kaimei New Material Technology Co., Ltd, Yueyang 414600, PR China*

Zhangyan Ma − *Key Laboratory of Chemical Biology & Traditional Chinese Medicine Research (Ministry of Education, China), College of Chemistry and Chemical Engineering, Hunan Normal University, Changsha 410081, PR China*

Peipei Li − *Key Laboratory of Chemical Biology & Traditional Chinese Medicine Research (Ministry of Education, China), College of Chemistry and Chemical Engineering, Hunan Normal University, Changsha 410081, PR China*

Youyu Zhang − *Key Laboratory of Chemical Biology & Traditional Chinese Medicine Research (Ministry of Education, China), College of Chemistry and Chemical Engineering, Hunan Normal University, Changsha 410081, PR China*; orcid.org/0000-0002-7502-6817

Shouzhuo Yao − *Key Laboratory of Chemical Biology & Traditional Chinese Medicine Research (Ministry of Education, China), College of Chemistry and Chemical Engineering, Hunan Normal University, Changsha 410081, PR China*

Complete contact information is available at: https://pubs.acs.org/10.1021/acs.jafc.1c01174

Notes

The authors declare no competing financial interest.

■ ACKNOWLEDGMENTS

This work was financially supported by the National Natural Science Foundation of China (21974042, 21904039, and 21645008), the Scientific Research Fund of Hunan Provincial Education Department (18A010), the Science and Technology Department of Hunan Province (14JJ4030 and 2020JJ5352), Hunan Provincial Science and Technology Department (2019RS5001), and Hunan province college students research learning and innovative experiment project (S201910542072 and 2019146).

■ REFERENCES

(1) El Sayed, S.; Pascual, L.; Licchelli, M.; Martínez-Máñez, R.; Gil, S.; Costero, A. M.; Sancenón, F. Chromogenic detection of aqueous formaldehyde using functionalized silica nanoparticles. *ACS Appl. Mater. Interfaces* **2016**, *8*, 14318−14322.

(2) Deng, L.; Liu, Q.; Lei, C.; Zhang, Y.; Huang, Y.; Nie, Z.; Yao, S. Fluorometric and colorimetric dual-readout assay for histone demethylase activity based on formaldehyde inhibition of Ag^+-triggered oxidation of o-phenylenediamine. *Anal. Chem.* **2020**, *92*, 9421−9428.

(3) Deng, Y.; Zhang, Q.; Zhang, H.; Zhang, C.; Wang, W.; Gu, Y. Kinetics of 3,4-dihydro-2H-3-phenyl-1,3-benzoxazine synthesis from mannich base and formaldehyde. *Ind. Eng. Chem. Res.* **2014**, *53*, 1933−1939.

(4) Atala, A. Re: Endogenous formaldehyde is a hematopoietic stem cell genotoxin and metabolic carcinogen. *J. Urol.* **2016**, *196*, 279−280.

(5) Cole, P.; Adami, H. O.; Trichopoulos, D.; Mandel, J. S. Re: Mortality from lymphohematopoietic malignancies and brain cancer among embalmers exposed to formaldehyde. *J. Natl. Cancer Inst.* **2010**, *102*, 1518−1519.

(6) Tong, Z.; Han, C.; Qiang, M.; Wang, W.; Lv, J.; Zhang, S.; Luo, W.; Li, H.; Luo, H.; Zhou, J.; Wu, B.; Su, T.; Yang, X.; Wang, X.; Liu, Y.; He, R. Age-related formaldehyde interferes with DNA methyltransferase function, causing memory loss in Alzheimer's disease. *Neurobiol. Aging* **2015**, *36*, 100−110.

(7) Deng, Z.; Hu, K.; Zhang, Y.; Zhao, W.; Wang, F.; Guo, L.; Zhang, W.; He, J.; Huang, Y.; Zhang, S. On-cartridge derivatisation using a calixarene solid-phase extraction sorbent for facile, sensitive and fast determination of formaldehyde in beer. *Food Chem.* **2016**, *211*, 314−319.

(8) Wahed, P.; Razzaq, M. A.; Dharmapuri, S.; Corrales, M. Determination of formaldehyde in food and feed by an in-house validated HPLC method. *Food Chem.* **2016**, *202*, 476−483.

(9) Zhang, Z.; Zhao, C.; Ma, Y.; Li, G. Rapid analysis of trace volatile formaldehyde in aquatic products by derivatization reaction-based surface enhanced Raman spectroscopy. *Analyst* **2014**, *139*, 3614−3621.

(10) Wei, J.; Chang, W.; Qileng, A.; Liu, W.; Zhang, Y.; Rong, S.; Lei, H.; Liu, Y. Dual-modal split-type immunosensor for sensitive

detection of microcystin-LR: enzyme-induced photoelectrochemistry and colorimetry. *Anal. Chem.* **2018**, *90*, 9606−9613.
(11) Zhu, X.; Li, J.; He, H.; Huang, M.; Zhang, X.; Wang, S. Application of nanomaterials in the bioanalytical detection of disease-related genes. *Biosens. Bioelectron.* **2015**, *74*, 113−133.
(12) Xiong, C.; Zhang, T.; Kong, W.; Zhang, Z.; Qu, H.; Chen, W.; Wang, Y.; Luo, L.; Zheng, L. ZIF-67 derived porous Co_3O_4 hollow nanopolyhedron functionalized solution-gated graphene transistors for simultaneous detection of glucose and uric acid in tears. *Biosens. Bioelectron.* **2018**, *101*, 21−28.
(13) Yan, Z.; Deng, P.; Liu, Y. Recent advances in protein kinase activity analysis based on nanomaterials. *Int. J. Mol. Sci.* **2019**, *20*, 1440−1451.
(14) Wang, Y.; Qu, K.; Tang, L.; Li, Z.; Moore, E.; Zeng, X.; Liu, Y.; Li, J. Nanomaterials in carbohydrate biosensors. *TrAC, Trends Anal. Chem.* **2014**, *58*, 54−70.
(15) Grattieri, M.; Minteer, S. D. Self-powered biosensors. *ACS Sens.* **2018**, *3*, 44−53.
(16) Katz, E.; Bückmann, A. F.; Willner, I. Self-powered enzyme-based biosensors. *J. Am. Chem. Soc.* **2001**, *123*, 10752−10753.
(17) Zhu, H.; Cai, Y.; Qileng, A.; Quan, Z.; Zeng, W.; He, K.; Liu, Y. Template-assisted Cu_2O@$Fe(OH)_3$ yolk-shell nanocages as biomimetic peroxidase: A multi-colorimetry and ratiometric fluorescence separated-type immunosensor for the detection of ochratoxin A. *J. Hazard. Mater.* **2021**, *411*, 125090−125101.
(18) Zhu, H.; Quan, Z.; Hou, H.; Cai, Y.; Liu, W.; Liu, Y. A colorimetric immunoassay based on cobalt hydroxide nanocages as oxidase mimics for detection of ochratoxin A. *Anal. Chim. Acta* **2020**, *1132*, 101−109.
(19) Li, H.; Wang, H.; Yang, M.; Sun, Y.; Yin, Y.; Guo, P. Mg-inserted δ-MnO_2 nanosheet assembly for enhanced energy storage. *Colloids Surf., A* **2020**, *602*, 125068−125077.
(20) Wei, W.; Cui, X.; Chen, W. Manganese oxide-based materials as electrochemical supercapacitor electrodes. *Chem. Soc. Rev.* **2011**, *40*, 1697−1721.
(21) Liu, Z.; Xu, K.; Sun, H.; Yin, S. One-step synthesis of single layer MnO_2 nanosheets with multi-role sodium dodecyl sulfate for high-performance pseudocapacitors. *Small* **2015**, *11*, 2182−2191.
(22) Xiao, T.; Sun, J.; Zhao, J.; Wang, S.; Liu, G.; Yang, X. FRET effect between fluorescent polydopamine nanoparticles and MnO_2 nanosheets and its application for sensitive sensing of alkaline phosphatase. *ACS Appl. Mater. Interfaces* **2018**, *10*, 6560−6569.
(23) Sheng, J.; Jiang, X.; Wang, L.; Yang, M.; Liu, Y.-N. Biomimetic mineralization guided one-pot preparation of gold clusters anchored two-dimensional MnO_2 nanosheets for fluorometric/magnetic bimodal sensing. *Anal. Chem.* **2018**, *90*, 2926−2932.
(24) Yang, Q.; Li, C.; Li, J.; Arabi, M.; Wang, X.; Peng, H.; Xiong, H.; Choo, J.; Chen, L. Chen., L. Multi-emitting fluorescence sensor of MnO_2-OPD-QD for the multiplex and visual detection of ascorbic acid and alkaline phosphatase. *J. Mater. Chem. C* **2020**, *8*, 5554−5561.
(25) Li, H.; Wang, Z.; Zhao, J.; Guan, Y.; Liu, Y. Dual colorimetric and ratiometric fluorescent responses for the determination of glutathione based on fluorescence quenching and oxidase-like activity of MnO_2 nanosheets. *ACS Sustainable Chem. Eng.* **2020**, *8*, 16136−16142.
(26) Chu, S.; Wang, H.; Du, Y.; Yang, F.; Yang, L.; Jiang, C. Portable smartphone platform integrated with a nanoprobe-based fluorescent paper strip: visual monitoring of glutathione in human serum for health prognosis. *ACS Sustainable Chem. Eng.* **2020**, *8*, 8175−8183.
(27) Gu, C.; Kong, X.; Yan, S.; Gai, P.; Li, F. Glucose dehydrogenase-like nanozyme based on black phosphorus nanosheets for high-performance biofuel cells. *ACS Sustainable Chem. Eng.* **2020**, *8*, 16549−16554.
(28) Zhang, Q.; Wang, F.; Zhang, H.; Zhang, Y.; Liu, M.; Liu, Y. Universal Ti_3C_2 MXenes based self-standard ratiometric fluorescence resonance energy transfer platform for highly sensitive detection of exosomes. *Anal. Chem.* **2018**, *90*, 12737−12744.
(29) Li, H.; Wang, Z.; Zhao, J.; Guan, Y.; Liu, Y. Dual colorimetric and ratiometric fluorescent responses for the determination of glutathione based on fluorescence quenching and oxidase-like activity of MnO_2 nanosheets. *ACS Sustainable Chem. Eng.* **2020**, *8*, 16136−16142.
(30) Ge, J.; Cai, R.; Chen, X.; Wu, Q.; Zhang, L.; Jiang, Y.; Cui, C.; Wan, S.; Tan, W. Facile approach to prepare HSA-templated MnO_2 nanosheets as oxidase mimic for colorimetric detection of glutathione. *Talanta* **2019**, *195*, 40−45.
(31) Shi, M.; Cen, Y.; Xu, G.; Wei, F.; Xu, X.; Cheng, X.; Chai, Y.; Sohail, M.; Hu, Q. Ratiometric fluorescence monitoring of α-glucosidase activity based on oxidase-like property of MnO_2 nanosheet and its application for inhibitor screening. *Anal. Chim. Acta* **2019**, *1077*, 225−231.
(32) Ma, Z.; Wu, T.; Li, P.; Liu, M.; Huang, S.; Li, H.; Zhang, Y.; Yao, S. A dual (colorimetric and fluorometric) detection scheme for glutathione and silver (I) based on the oxidase mimicking activity of MnO_2 nanosheets. *Microchim. Acta* **2019**, *186*, 498−507.
(33) Mandal, M.; Nagaraju, V.; Karunakar, G. V.; Sarma, B.; Borah, B. J.; Bania, K. K. Electronic, conjugation, and confinement effects on structure, redox, and catalytic behavior of oxido-Vanadium (IV) and -(V) chiral Schiff base complexes. *J. Phys. Chem. C* **2015**, *119*, 28854−28870.
(34) Liu, J.; Wei, Y.; Li, P.-Z.; Zhang, P.; Su, W.; Sun, Y.; Zou, R.; Zhao, Y. Experimental and theoretical investigation of mesoporous MnO_2 nanosheets with oxygen vacancies for high-efficiency catalytic $DeNO_x$. *ACS Catal.* **2018**, *8*, 3865−3874.
(35) Ma, K.; Liang, L.; Zhou, X.; Tan, W.; Hu, O.; Chen, Z. A Redox-induced dual-mode colorimetric and fluorometric method based on N-CDs and MnO_2 for determination of isoniazid in tablets and plasma samples. *Spectrochim. Acta, Part A* **2021**, *247*, 119097−119103.
(36) Sheng, J.; Jiang, X.; Wang, L.; Yang, M.; Liu, Y.-N. Biomimetic Mineralization Guided One-Pot Preparation of Gold Clusters Anchored Two-Dimensional MnO_2 Nanosheets for Fluorometric/Magnetic Bimodal Sensing. *Anal. Chem.* **2018**, *90*, 2926−2932.
(37) Wan, K.; Wang, D.; Wang, F.; Li, H.; Xu, J.; Wang, X.; Yang, J. Hierarchical In_2O_3@SnO_2 core-shell nanofiber for high efficiency formaldehyde detection. *ACS Appl. Mater. Interfaces* **2019**, *11*, 45214−45225.
(38) Zhai, B.; Zhang, Y.; Hu, Z.; He, J.; Liu, J.; Gao, C.; Li, W. A ratiometric fluorescent probe for the detection of formaldehyde in aqueous solution and air via Aza-Cope reaction. *Dyes Pigm.* **2019**, *171*, 107743−107772.
(39) Zhang, X.; Sun, Y.; Fan, Y.; Liu, Z.; Zeng, Z.; Zhao, H.; Wang, X.; Xu, J. Effects of organotin halide perovskite and Pt nanoparticles in SnO_2-based sensing materials on the detection of formaldehyde. *J. Mater. Sci.: Mater. Electron.* **2019**, *30*, 20624−20637.
(40) Zhou, W.; Dong, H.; Yan, H.; Shi, C.; Yu, M.; Wei, L.; Li, Z. HCHO-reactive molecule with dual-emission-enhancement property for quantitatively detecting HCHO in near 100% water solution. *Sens. Actuators, B* **2015**, *209*, 664−669.
(41) Zhao, X.; Ji, C.; Ma, L.; Wu, Z.; Cheng, W.; Yin, M. An aggregation-induced emission-based "Turn-On" fluorescent probe for facile detection of gaseous formaldehyde. *ACS Sens.* **2018**, *3*, 2112−2117.
(42) Zong, J.; Zhang, Y. S.; Zhu, Y.; Zhao, Y.; Zhang, W.; Zhu, Y. Rapid and highly selective detection of formaldehyde in food using quartz crystal microbalance sensors based on biomimetic polydopamine functionalized hollow mesoporous silica spheres. *Sens. Actuators, B* **2018**, *271*, 311−320.
(43) Kundu, M.; Bhardwaj, H.; Pandey, M. K.; Krishnan, P.; Kotnala, R. K.; Sumana, G. Development of electrochemical biosensor based on CNT-Fe_3O_4 nanocomposite to determine formaldehyde adulteration in orange juice. *J. Food Sci. Technol.* **2019**, *56*, 1829−1840.
(44) Chaiendoo, K.; Sooksin, S.; Kulchat, S.; Promarak, V.; Tuntulani, T.; Ngeontae, W. A new formaldehyde sensor from silver nanoclusters modified Tollens' reagent. *Food Chem.* **2018**, *255*, 41−48.

https://doi.org/10.1021/acs.jafc.1c01174
J. Agric. Food Chem. 2021, 69, 7303−7312

(45) Tsuchiya, K.; Furusawa, H.; Nomura, A.; Matsui, H.; Nihei, M.; Tokito, S. Formaldehyde detection by a combination of formaldehyde dehydrogenase and chitosan on a sensor based on an organic field-effect transistor. *Technologies* **2019**, *7*, 48−55.
(46) Zhu, L.; Jacob, D. J.; Keutsch, F. N.; Mickley, L. J.; Scheffe, R.; Strum, M.; González Abad, G.; Chance, K.; Yang, K.; Rappenglück, B.; Millet, D. B.; Baasandorj, M.; Jaeglé, L.; Shah, V. Formaldehyde (HCHO) As a Hazardous Air Pollutant: Mapping Surface Air Concentrations from Satellite and Inferring Cancer Risks in the United States. *Environ. Sci. Technol.* **2017**, *51*, 5650−5657.

https://doi.org/10.1021/acs.jafc.1c01174
J. Agric. Food Chem. 2021, 69, 7303−7312